

## Growth of Si on the Si(111) surface

C. J. Lanczycki, R. Kotlyar, E. Fu, Y.-N. Yang, E. D. Williams, and S. Das Sarma

*Department of Physics, University of Maryland, College Park, Maryland 20742-4111*

(Received 24 March 1997; revised manuscript received 15 September 1997)

The homoepitaxial growth of Si on a Si(111) surface for  $T=280-410^\circ\text{C}$ , and thicknesses up to 210 bilayers has been evaluated using scanning tunneling microscopy and detailed statistical analyses. In the early stages of growth, the formation of and nucleation at antiphase domain boundaries and the formation of metastable crystalline structures become increasingly important at lower temperatures. At larger film thickness, the height-height correlation functions do not reveal the presence of scale-invariant morphologies. Instead, anomalous formation of pyramidal structures with surrounding denuded zones is observed at temperatures of  $360^\circ\text{C}$  and below. The pyramid size increases with increasing temperature and film thickness, but this increase is not consistent with a simple coarsening process. Atomic-scale images indicate a correlation of these pyramids with the metastable crystalline structures observed in growth nuclei at lower coverages. Potential mechanisms for formation of these anomalous structures and their consequences for scale-invariant growth are discussed. Our results indicate that the underlying crystal structure and its associated reconstructions can play a significant role in determining surface growth morphologies, complicating their long-wavelength dynamic scaling properties. [S0163-1829(98)00716-4]

### I. INTRODUCTION

The key concept in kinetic surface roughening is that of statistical scale invariance, which asserts that, at long enough length and time scales, nonequilibrium growth of thin films should exhibit dynamic scaling in length and time because there are no characteristic scales in the problem. For many years, there has been a coordinated effort to develop a theoretical description of film growth in which the large-scale evolution of structure could be described in terms of a few key parameters that subsume all of the detailed atomistic behavior of a given individual material.<sup>1-5</sup> Additionally, many attempts to model these processes have employed very detailed simulations,<sup>6</sup> or focused on the layer-by-layer growth regime.<sup>7</sup> With the identification of kinetic roughening as a scale-invariant phenomenon,<sup>1,2</sup> much simpler models became relevant to the asymptotic properties of kinetically rough surfaces. Interfaces undergo kinetic roughening whenever the adatoms deposited by an incident beam diffuse slowly as compared to the deposition rate, so that they do not reach equilibrium positions. Generically, kinetic roughening manifests scale invariance, which can be characterized by theory based only on the presence of a noisy incident beam and the nature of physical processes occurring during growth. At first, these models neglected surface diffusion effects following deposition.<sup>8</sup> Later developments have allowed the appropriate incorporation of surface diffusional processes,<sup>3-5</sup> with a correlated improvement in the ability of theory to describe the evolution of global structure.

However, experimental studies increasingly reveal<sup>9-13</sup> that the complexities of surface diffusion can lead to the evolution of kinetically rough surfaces that display scale invariance characterized by a range of exponents. In addition, an Ehrlich-Schwoebel-type barrier<sup>14,15</sup> to diffusion downwards across a step can have dramatic effects on growth morphology and obscure noise-driven roughening effects. Such barriers have been studied experimentally,<sup>10-12</sup>

simulationally,<sup>7,16</sup> and theoretically.<sup>5,11,12,17,18</sup> They lead to interfaces with mound or pyramidal structures where a coarsening-type phenomenon dominates. The appropriate incorporation of such specific diffusional behavior into dynamical scaling formalisms remains a theoretical challenge.

Growing kinetically rough surfaces have often been taken as examples of self-affine objects, which possess the behavior that on “short” length scales they appear rough while measurements at “larger” scales find the surface to be flat. This implies anisotropic scale invariance, whereby distances measured normal to the substrate scale as  $h \rightarrow f^\alpha h$  ( $\alpha < 1$ ) when lengths measured in the plane of the initial substrate are rescaled as  $L \rightarrow fL$ . Physically, we note that the length scale at which the crossover from rough to flat occurs can be taken as the lateral correlation length  $\xi(t)$ : on local scales  $r$  such that  $r \ll \xi$ , the surface looks spatially rough, while for  $r \gg \xi$  it appears globally flat. Note that all of these discussions tacitly assume that the length scale defining the crystallinity of the surface are very small compared to  $\xi(t)$ .

The power-law scaling implied by these ideas defines a set of scaling exponents. The roughness exponent  $\alpha$  describes the spatial scaling, and the growth exponent  $\beta$  characterizes the time development of the height fluctuations. The dynamical exponent  $z = \alpha/\beta$  describes the spread of lateral correlations:  $\xi(t) \sim t^{1/z}$ . We note an implicit  $T$  dependence in the growth characteristics due to the activated nature of adatom diffusion, and the influence of finite size and time effects.<sup>19</sup> Because  $\xi$  defines the length and time regimes over which scaling behavior can be observed, it is crucial to know the correlation length relative to the length scales being probed.

Most frequently one obtains the exponents from the height-height correlation function  $G(\vec{x}, t) = \langle [h(\vec{x} + \vec{y}, t) - h(\vec{x}, t)]^2 \rangle^{1/2}$ , and the interface width  $W(R, t)$ , where  $\langle \cdots \rangle$  is an average over all surface vectors  $\vec{y}$  and  $R$  is the lateral length scale over which the average height fluctua-

tions are computed. For anisotropic, self-affine scale invariance where  $\alpha < 1$ , one expects the scaling  $G(x) \sim x^\alpha$  and  $W(R) \sim R^\alpha$  for  $x, R < \xi(t)$ . Since  $G$  and  $W$  depend on time, scale invariance also demands that both  $G(t)$  and  $W(t) \sim t^\beta$  for  $x, R > \xi(t)$ . From the point of view of self-affine scaling, then,  $G$  and  $W$  provide equivalent information. We primarily discuss data from the correlation function, but  $W$  has also been examined and yields the same results. We note that situations exist where the growth can obey an anomalous scaling law (in contrast to the usual self-affine scaling).<sup>20</sup> Experimentally, growing surfaces have been seen to exhibit temporal and spatial power-law scaling behavior during low-temperature growth.<sup>9–13</sup> Using real-space scanning tunneling microscopy (STM) images, we can directly examine whether surfaces exhibit this scaling as the interface evolves.<sup>21–24</sup>

In this paper, we study the growth of Si on Si(111) with step separations  $> 2000$  Å and over a temperature range of approximately 280–410 °C where atoms exhibit relatively slow surface diffusion and could be expected to lead to kinetic roughening.<sup>13,25–34</sup> Due to the activated Arrhenius nature of surface diffusion, the mobility changes rapidly with temperature. We use STM along with extensive statistical image analyses of our experiments. We find that while the surface grows primarily via layer-by-layer island growth, small portions of the surface are covered with tall quasipyramidal structures (except at  $T = 410$  °C). These structures have morphologies and microcrystallinities strongly resembling the structures formed at low coverages during nucleation at antiphase boundaries.<sup>25</sup> As temperature is decreased, the number of these structures increases, while their typical size decreases.<sup>35</sup>

The Si/Si(111) system, however, is far from simple. In particular, the surface undergoes a complex large-scale reconstruction, which differs only slightly in energy from many other metastable reconstructive structures.<sup>36,37</sup> Previous studies have shown that the antiphase domain boundaries of the surface reconstruction act as nucleation sites for growth.<sup>25</sup> Furthermore, islands nucleating at these domain boundaries are likely to form in one of the metastable reconstructions,<sup>36,37</sup> leading to the formation of additional domain boundaries during subsequent growth.<sup>25,32</sup> This perturbation of the normal random nucleation process in growth represents a potentially interesting challenge to theories of the evolution of morphology, particularly those involving dynamic scaling approaches. Specifically, these processes introduce new length scales in the problem that are substantially larger than atomistic lattice spacings, e.g., the  $7 \times 7$  reconstruction unit cell on the Si(111) surface. This new length scale complicates the interpretation of the growing surface morphology in terms of dynamically scaling kinetic roughening.

Global statistical measures such as the width  $W$  and lateral correlation length  $\xi$  can be used to gauge whether or not the machinery of dynamic scaling should be relevant to a given surface. In particular, we would minimally expect that (a) the surface width  $W \geq c$ , where  $c$  is the height of a single monolayer [ $c = 3.14$  Å on the Si(111)  $7 \times 7$  surface], and (b) the correlation length is  $\xi \approx 10a$  or greater, with  $a$  being the size of the basic unit cell [ $a = 30$  Å for the  $7 \times 7$  Si(111) reconstruction]. To our mind, fluctuations of less than a single layer or spanning distances of but a few underlying

cells cannot reliably confirm the presence of dynamic scaling.

Our results supplement existing experimental results at a nominal temperature slightly below our lowest quoted temperature,  $T = 280$  °C. The previous experiments, performed by Yang, Wang, and Lu using electron diffraction techniques,<sup>13</sup> studied Si/Si(111) growth at  $T = 275$  °C with a flux of seven bilayers/min for times up to 20 min. With an extensive HRLEED (high-resolution low-energy electron diffraction) study of the grown surfaces, they found scaling exponents of  $\alpha \sim 1.0$ ,  $\beta \sim 1/4$ , and the average terrace size grew as  $\sqrt{\ln t}$ . These observations suggests very rough growth of the interface consistent with the anomalous scaling behavior<sup>20</sup> manifested by the linear stochastic Herring-Mullins equation describing the surface diffusion of atoms on a growing interface:<sup>3</sup>  $\partial h / \partial t = -\nu \nabla^4 h + D$ , where  $D$  is a stochastic term representing the shot noise in the incident atomic beam. We note that at  $T = 275$  °C, their growth does satisfy the minimal criteria for kinetic roughening noted above. But in growth at  $T = 350$  °C, they found layer-by-layer growth with no kinetic roughening.<sup>13</sup> Our STM data complement those of Ref. 13 by focusing on the transitional temperature regime starting just above 275 °C (where Yang saw roughening and dynamic scaling) and considering the crossover from this to smooth layer-by-layer growth. We examine this issue on morphological grounds and from the point of view of statistical scale invariance. Taken together, these data show that the roughening of the Si(111) surface is quite temperature dependent, and that above 275 °C a rapid transition to layer-by-layer growth occurs.

Yang, Wang, and Lu<sup>33</sup> also observed that if they intentionally roughened the surface on a length scale less than about 100 Å prior to growth, the LEED pattern developed features characteristic of (112) and (113) facets after the deposition of many layers of Si. Under these roughened growth conditions the original  $7 \times 7$  reconstruction disappeared after several layers of growth. The facet features reported under such growth conditions<sup>33</sup> are much better ordered and probably much larger than the quasipyramidal structures we observe. In addition, Shigeta *et al.* have reported the formation of hillocks during a growth regime in which initial RHEED oscillations had damped out.<sup>35</sup>

In contrast to the characteristic coarsening of pyramids or mounds expected due to Ehrlich-Schwoebel barriers,<sup>12,17</sup> we do not see any interface coarsening in our experimental results despite the appearance of small isolated patches displaying pyramidal structures. We attribute the appearance of pyramidal structures in our experiments to metastable reconstructions at antiphase domain boundaries as explained later in this article.

## II. EXPERIMENT

The experiments were performed in an UHV system with a base pressure of  $2 \times 10^{-11}$  torr, equipped with a homemade scanning tunneling microscope.<sup>23</sup> Nominally flat Si(111),  $n$ -type wafers of resistivity 10–30 Ω cm and  $15 \times 3 \times 0.4$  mm<sup>3</sup> in size were used as samples. Clean Si(111) surfaces (without any chemical precleaning) were obtained by flashing to 1270 °C for one minute, after slowly degassing the sample at temperatures below 945 °C. Depending on the

direction of the direct current during the flash, step up or step down, the sample substrate had either uniform terraces  $\sim 2000$  Å wide or had direct-current-induced step bunching.<sup>38</sup> On the step-bunched samples, growth was studied on the terraces between the step bunches, where steps crossing between the bunches yield an average step separation of 1–2  $\mu\text{m}$ . From 1270 °C, the samples were cooled quickly to 945 °C and then slowly cooled to below 250 °C at a rate of  $\sim 0.5$  °C/s to produce a surface with few domain boundaries.<sup>25</sup> Another Si(111) wafer placed  $\sim 2$  cm from the sample is used as the Si deposition source. The deposition rate in these studies was approximately seven bilayers per minute and was calibrated by performing depositions on step-bunched samples with wide terraces. On such samples at temperatures where growth is primarily by island formation, one can directly observe the amount of Si deposited using STM. The images clearly show denuded zones around the step bunches (where deposited material has traveled primarily to the step edges) and islands in the central regions of the terraces. For submonolayer deposition, the area covered by the islands gives the amount deposited onto the regions of the surface outside the denuded zones, and thus give a direct calibration of the deposition flux accurate to better than 10% (error arises primarily from defining the edge of the denuded zones.) The pressure during the deposition was less than  $4 \times 10^{-11}$  torr. The coverage due to deposition is expressed in units of bilayers (BL) of Si(111) where 1 BL is equal to  $1.36 \times 10^{15}$  atoms/cm<sup>2</sup>.

Temperatures were calibrated using an optical pyrometer at elevated temperature, and an infrared pyrometer down to approximately 400 °C. Below 400 °C the temperature was extrapolated using the variation in the current used to heat the sample. As a result, systematic uncertainties in the temperatures reported of  $\pm 40$  °C at 280 °C and  $\pm 50$  °C at 410 °C are possible. As will be discussed later, by comparison with the work in Ref. 13, we conclude that for the same physical conditions our temperature calibration yields absolute numerical values approximately 10–20 degrees lower than they would be on the temperature scale of Yang, Wang, and Lu. (Our quoted experimental temperatures are based on our calibration, but when comparing with Ref. 13 it is important to factor in this difference.) Uncertainties in our relative temperatures are governed by uncertainties in the current measurement, and are less than  $\pm 10$  °C at the lowest temperature, and less than  $\pm 5$  °C at the highest growth temperature.

An STM scan of a surface provides the surface height data with respect to an image-dependent reference. To convert the raw STM output to an absolute height measure of the Si(111) surface we first performed a planar background subtraction on the data to compensate for any tilt of the substrate with respect to the STM tip. To convert the raw data into absolute height units we next averaged roughly 10 line scans of the surface, computing the mean height difference between adjacent regions showing a  $7 \times 7$  reconstruction on either side of a surface step. Our unit of height throughout this paper is the vertical lattice constant of the  $7 \times 7$  reconstruction,  $c = 3.14$  Å.

To characterize the distribution of atoms at the surface we sampled the height for each image and computed the probability  $P(h)$  of finding a surface point within the  $h$ th layer of

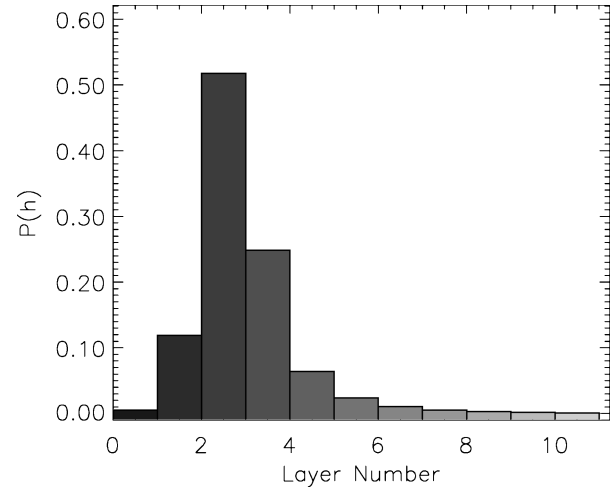


FIG. 1. Histogram plot of the image in Fig. 5(a), giving the probability  $P(h)$  that a random surface point is at height  $h$ .

the image. We show a typical histogram in Fig. 1 for a  $500 \times 500$  nm<sup>2</sup> STM image after a total of 210 BL was deposited at  $T = 320$  °C. From these histograms we extracted the likelihood of finding an arbitrary surface point in the three most probable layers, as given in Table I. As is clear from Table I the growth realized in our experiments leads to surfaces with atoms predominantly residing in three layers (i.e., the typical interface width  $W$  here is  $\sim 1$  BL), even in the presence of the pyramid formation, which will be described in the following section.

The surface regions, which appear as mounds or pyramids in the images, are defined and characterized by the following guidelines. We considered a region of connected surface points to be a mound if its maximum height is within  $H_r\%$  of the reference maximum height of a mound, its area is within  $A_r\%$  of the reference area of a mound, and its base is within  $B_r\%$  of the reference base of a mound. The optimal parameters  $H_r$ ,  $A_r$ , and  $B_r$  were determined empirically for each image, but on the average these values are  $H_r = 30\%$ ,  $A_r = 40\%$ , and  $B_r = 15\%$ . To determine these reference parameters we randomly selected several regions that exhibited mound formation in the image and calculated their area and height. The ensemble-averaged parameters were used as reference values when we analyzed the entire surface. We show these results in Table II where each entry includes the total number of mounds in the image, the fraction of the surface covered by the mounds, the average area of the mound, and the average maximum height ( $\bar{h}_m$ ) of the mound. As is evident from Table II the character of the mounds depends non-trivially on both the deposition time and the temperature of the substrate. In general, the mounds grow in area with increasing temperature and deposition time. The density of mounds in the images, however, decreases with increasing temperature. Although not determined conclusively, we observe that the  $\bar{h}_m$  values seem to be insensitive to the growth temperature for a fixed number of deposited layers.

We have used our STM images to calculate a predicted diffraction profile where we numerically evaluate the scattered intensity  $I(\vec{k}_{\parallel}, k_{\perp})$  as

TABLE I. Histogram analysis of  $500 \times 500 \text{ nm}^2$  images. Based on the vertical lattice spacing  $c$ , we give the total layers visible in the image ( $N_L$ ) and the percentage of the surface in the one, two, and three most probable layers ( $P_1, P_2, P_3$ , respectively).

Film thickness	$T = 280 \text{ }^\circ\text{C}$	$T = 320 \text{ }^\circ\text{C}$	$T = 360 \text{ }^\circ\text{C}$	$T = 410 \text{ }^\circ\text{C}$
30 BL	No data	$N_L = 9.5$ $P_1 = 49\%$ $P_2 = 75\%$ $P_3 = 93\%$	$N_L = 7$ $P_1 = 40\%$ $P_2 = 77\%$ $P_3 = 98\%$	$N_L = 2$ $P_1 = 62\%$ $P_2 = 100\%$ $P_3 = 100\%$
52 BL ( $T = 280 \text{ }^\circ\text{C}$ ) 67 BL ( $T = 360 \text{ }^\circ\text{C}$ )	$N_L = 11.5$ $P_1 = 52\%$ $P_2 = 75\%$ $P_3 = 94\%$	No data	$N_L = 8.9$ $P_1 = 87\%$ $P_2 = 97\%$ $P_3 = 99\%$	No data
105 BL	<sup>a</sup> $N_L = 9.3$ $P_1 = 49\%$ $P_2 = 79\%$ $P_3 = 92\%$	$N_L = 11$ $P_1 = 41\%$ $P_2 = 81\%$ $P_3 = 90\%$	No data	No data
210 BL	No data	$N_L = 11.2$ $P_1 = 52\%$ $P_2 = 77\%$ $P_3 = 89\%$	$N_L = 9.9$ $P_1 = 42\%$ $P_2 = 75\%$ $P_3 = 92\%$	$N_L = 3.6$ $P_1 = 51\%$ $P_2 = 99\%$ $P_3 = 100\%$

<sup>a</sup>See Ref. 43.

$$I(\vec{k}_\parallel, k_\perp) = \left| \sum_x e^{i\vec{k}_\parallel \cdot \vec{x}} \langle \exp[ik_\perp (h(\vec{x} + \vec{x}') - h(\vec{x}'))] \rangle \right|, \quad (1)$$

where  $\vec{k}_\parallel$  is the parallel wave-vector transfer to the surface,  $k_\perp$  is the perpendicular wave-vector transfer (always taken at the out-of-phase condition, namely,  $ck_\perp = (2n - 1)\pi, n = 0,$

$\pm 1, \pm 2, \dots$ ), and  $\langle \dots \rangle$  represents an ensemble average over pairs of points separated by the vector  $\vec{x}$  in the STM image. It has been shown<sup>39,40</sup> that near the out-of-phase condition the full width at half maximum (FWHM) of the intensity profile can be expressed as  $\text{FWHM} \sim 6\pi/\eta c$  where  $\eta$  is proportional to the average terrace size. It can be further written as  $\eta \sim \xi W^{-1/\alpha}$ ,<sup>41</sup> and in the case where  $\alpha = 1$  (as in Ref. 13)  $\eta \sim \xi/W$ . Since  $\eta$  in our case is nonuniform during much of the growth, and especially near the mounds, these

TABLE II. Characterization of the pyramidal structures, obtained from  $500 \times 500 \text{ nm}^2$  STM images. The number of pyramids observed, together with their average height ( $h_{\text{av}}$ ), average area covered per pyramid, and average surface coverage are shown, computed as described in the text.

Film thickness	$T = 280 \text{ }^\circ\text{C}$	$T = 320 \text{ }^\circ\text{C}$	$T = 360 \text{ }^\circ\text{C}$	$T = 410 \text{ }^\circ\text{C}$
30 BL	No data	None observed	None observed	None observed
52 BL ( $T = 280 \text{ }^\circ\text{C}$ ) 67 BL ( $T = 360 \text{ }^\circ\text{C}$ )	Sample: 18 $h_{\text{av}} = 4.0c$ Area = $125 \text{ nm}^2$ Coverage = 0.9%	No data	Sample: 3 $h_{\text{av}} = 3.7c$ Area = $1280 \text{ nm}^2$ Coverage = 1.5%	No data
105 BL	<sup>a</sup> Sample: 18 $h_{\text{av}} = 4.8c$ Area = $360 \text{ nm}^2$ Coverage = 2.5%	Sample: 13 $h_{\text{av}} = 4.8c$ Area = $450 \text{ nm}^2$ Coverage = 2.3%	No data	No data
210 BL	No data	Sample: 9 $h_{\text{av}} = 6.8c$ Area = $2250 \text{ nm}^2$ Coverage = 10%	Sample: 4 $h_{\text{av}} = 6.7c$ Area = $7350 \text{ nm}^2$ Coverage = 10%	None observed

<sup>a</sup>See Ref. 43.

relations most likely are not strictly valid. However, the physical expectation still is that the FWHM of the diffraction beam profile increases with surface width and decreases with increasing correlation length.

### III. RESULTS

#### A. Discussion of STM images

Growth was studied at room temperature, and at  $T=280$ , 320, 360, and 410 °C. The structures grown at room temperature, although apparently quite rough, were not analyzed because the STM images could not be interpreted due to a lack of recognizable crystal features, consistent with other reports of amorphous growth below about 200 °C.<sup>42</sup> Of course, one could still go ahead and conduct an analysis of the STM images obtained, but in our opinion such an analysis is not meaningful. Without identifying landmarks that indicate the presence of an actual crystal structure on the surface, it is unclear to what extent tip effects (including multiple tips and tip changes during a scan) are convolved with the true surface structure. Therefore, we do not present data obtained following room-temperature growth.

To investigate the effect of temperature on the growth we have compared the structure of relatively thin films (30 and 52 BL) grown at four temperatures (Fig. 2). The results are qualitatively as expected: island size (surface width) increases (decreases) with increasing temperature, with a concomitant rise in the diffusion length (qualitatively manifested by the distance between nucleating islands in the figures). At 320 °C, the island size is small, on the order of 100 Å in size. A histogram analysis (see Table I) shows that 93% of the surface is covered by the three most probable layers, with up to nine different layers exposed in the entire image at  $T=320$  °C. With increasing temperature, the lateral feature size increases and the number of layers that are simultaneously visible decreases. At  $T=410$  °C, virtually all of the growth is limited to two layers as expected for perfect layer-by-layer growth. Even at the lowest temperature ( $T=280$  °C, where roughness should be greatest), Fig. 2(a) displays many small features spanning mainly three layers with little global roughening evident.

Magnification of the same surfaces shows the atomic nature of the growing film [Figs. 3(a) and (b)]. The films grown at  $T=280$  and 320 °C still have crystalline order, but there are many domain boundaries and regions of metastable reconstructions, such as  $2\times 1$  and  $5\times 5$ , in addition to the normal  $7\times 7$  structure. Similar structures occur after growth at 360 °C as shown in Fig. 3(c), but with a larger length scale for the defect structure. Structures grown at  $T=410$  °C (not shown) continue this pattern, and appear similar to those reported previously in studies of nucleation at domain boundaries.<sup>25</sup>

With increasing coverage, we expect the evolution of a scale-invariant morphology most clearly at our lower temperatures. As we raise the temperature, we hope to illuminate how the Si/Si(111) surface crosses over to a layer-by-layer growth mode from a kinetically rough mode, with the results of Ref. 13 at  $T=275$  (350) °C being an example of the latter (former) mode. However, the morphological evolution we find at temperatures just above  $T=275$  °C (where we emphasize the temperature calibration uncertainties noted in

Sec. II) is uniformly quite different from what we expect of a scale-invariant kinetically rough surface. Namely, it should manifest fluctuations and substructures of a variety of heights and lateral extents.

At  $T=280$  and 320 °C though [Figs. 4(a) and (b), respectively], large regions of the surface remain surprisingly flat and dominated by only two or three layers.<sup>43</sup> But these flat regions are punctuated by the appearance of much taller pyramidal structures. These pyramids are basically triangular in cross section and are surrounded by a zone denuded of any island structures. Heights lower than those of the surrounding flat areas are typically found in the denuded zones. A line scan of Fig. 4(b) appears in Fig. 5(a) and clearly shows the existence of a large layered structure amidst the background of a relatively flat surface. The observation at  $T=360$  °C [Fig. 4(c)] is similar except that there are fewer pyramids of larger size. Finally, at  $T=410$  °C [Fig. 4(d)] the film appears uniformly smooth, and essentially identical to that observed after 30 BL of growth [Fig. 2(d)]. The corresponding line scan at  $T=410$  °C [Fig. 5(b)] confirms that only two layers are active at our highest temperature. While the overlayer chiefly forms a  $7\times 7$  structure, one can also detect areas of  $2\times 1$  reconstruction, as seen in Fig. 4(e).

Although the pyramidal structures formed at  $T=320$  and 360 °C are visually dramatic, the analysis of the height distribution in Table I illustrates that the majority of the surface structure is composed of flat regimes, and the entire image is largely limited to three layers (89% at  $T=320$  °C, and 92% at 360 °C). An analysis of the pyramidal structures themselves, presented in Table II, shows that after 210 BL of growth they cover approximately 10% of the surface area, and have an average maximum height of about seven layers ( $\sim 22$  Å) above the overall surface average. As observed visually in Fig. 6, qualitatively the pyramids are of larger size and fewer in number at elevated temperatures.

The characteristics of the islands can be further understood by imaging the same surfaces at different magnifications. Larger area images are shown in Fig. 6. These 2- $\mu\text{m}$ -size images show that the pyramidal structures are uniformly distributed over the surface, and have a relatively narrow distribution of size. Comparison of the growth patterns under the same conditions on the substrates of different step density described in the experimental section showed no qualitative difference in the distribution of the pyramid structures formed. Finally, at our highest growth temperature of  $T=410$  °C [Fig. 6(c)], there is no evidence at all of any pyramid formation, or the presence of structures that could be considered an early stage of a pyramidal structure. This observation is consistent with the lack of kinetic roughening at high temperature found previously for Si/Si(111) growth.<sup>13</sup>

The atomic-scale structure of the pyramids is illustrated in the high-magnification images shown in Fig. 7. The filtered images clearly show that the pyramids maintain the atomic reconstructions characteristic of the Si(111) surface, and have a structure that is aligned with the high-symmetry directions of the surface. The ‘pyramidal’ shape, however, is not a true pyramid but appears to be the result of the growth of tall thin walls aligned along each of the three high-symmetry directions. There is considerable variability in the

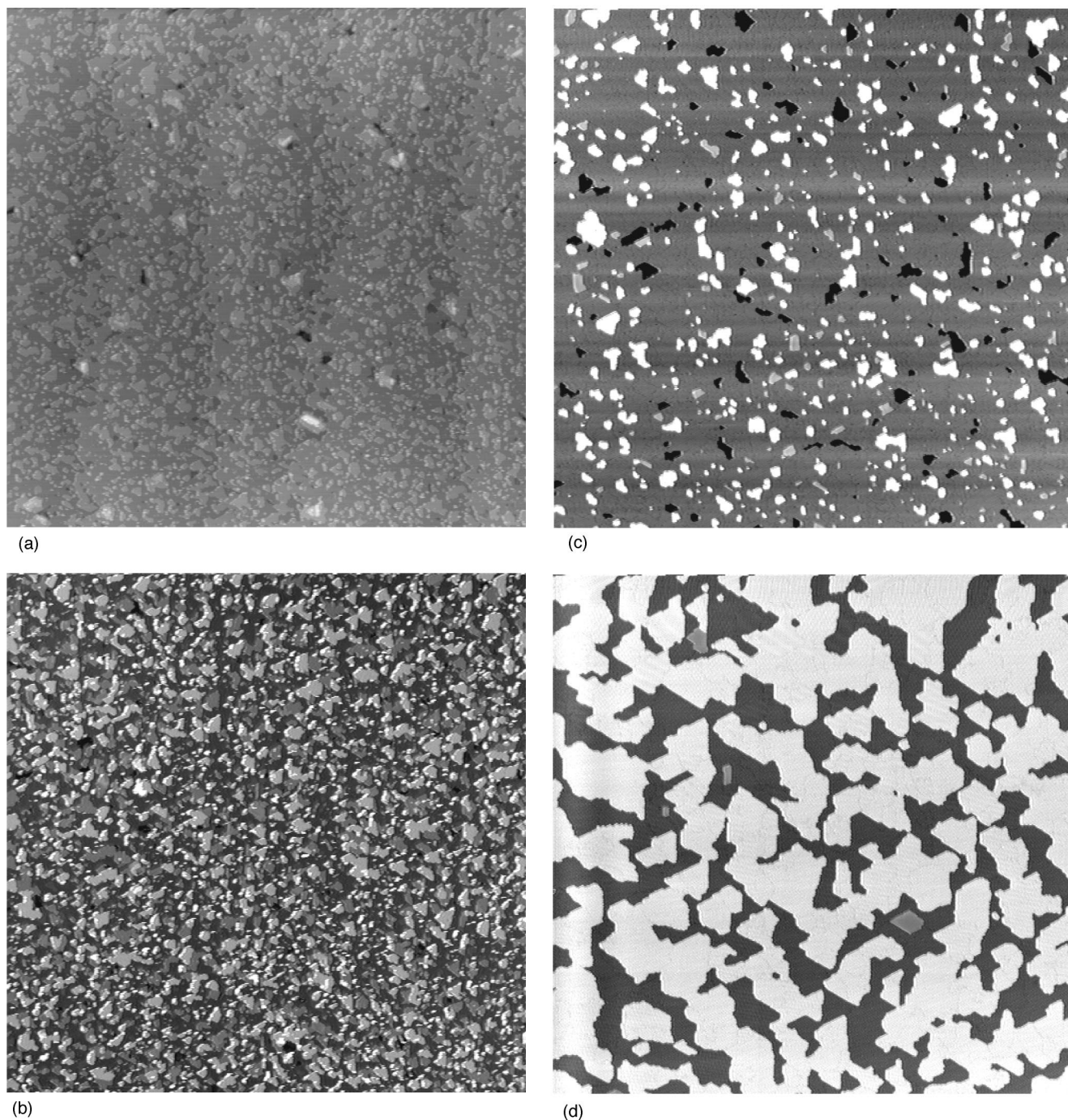


FIG. 2.  $5000 \times 5000 \text{ \AA}$  STM images following deposition of (a) 52 BL of Si at  $T=280^\circ\text{C}$ , and 30 BL of Si at (b)  $T=320^\circ\text{C}$ , (c)  $T=360^\circ\text{C}$ , (d)  $T=410^\circ\text{C}$ . In (c) and (d) the islands with intermediate shading possess the metastable  $2 \times 1$  structure.

shapes of the pyramids as can be seen in Fig. 4. However, the “hollow” structure shown in Figs. 7(a) and 7(b) is quite common. The structure shown in Figs. 7(c) and 7(d) shows another pyramid composed of what appear to be rows of parallel ridges that have grown together, yet with an overall shape similar to that in Figs. 7(a) and 7(b).

Under all the conditions reported, we continue to observe well-defined crystalline structures, including the  $7 \times 7$  reconstruction and the related metastable  $n \times n$  reconstructions, and the  $2 \times 1$  reconstruction. Small structures displaying multiple layers of different reconstructions could be found at thicknesses as small as 20 BL for  $T=360^\circ\text{C}$ , as shown in

Fig. 8(a), and were also observed on thicker films as shown in Fig. 8(b). Following 67 BL of deposition, well-defined pyramid-type structures [as seen in Fig. 7(c)] were observed at the three lowest temperatures studied. The structures all tend to show the same symmetry as seen in Figs. 4 and 7, in which the “pyramids” are formed of three (or parts of three) long thin walls oriented along the high-symmetry directions. The overall nature of the structures observed in the varying stages of growth thus suggests that their growth does not result from the evolution of an initial triangular shaped island. Rather, they may be the result of growth from the long thin islands of the metastable  $2 \times 1$  reconstruction, visible in

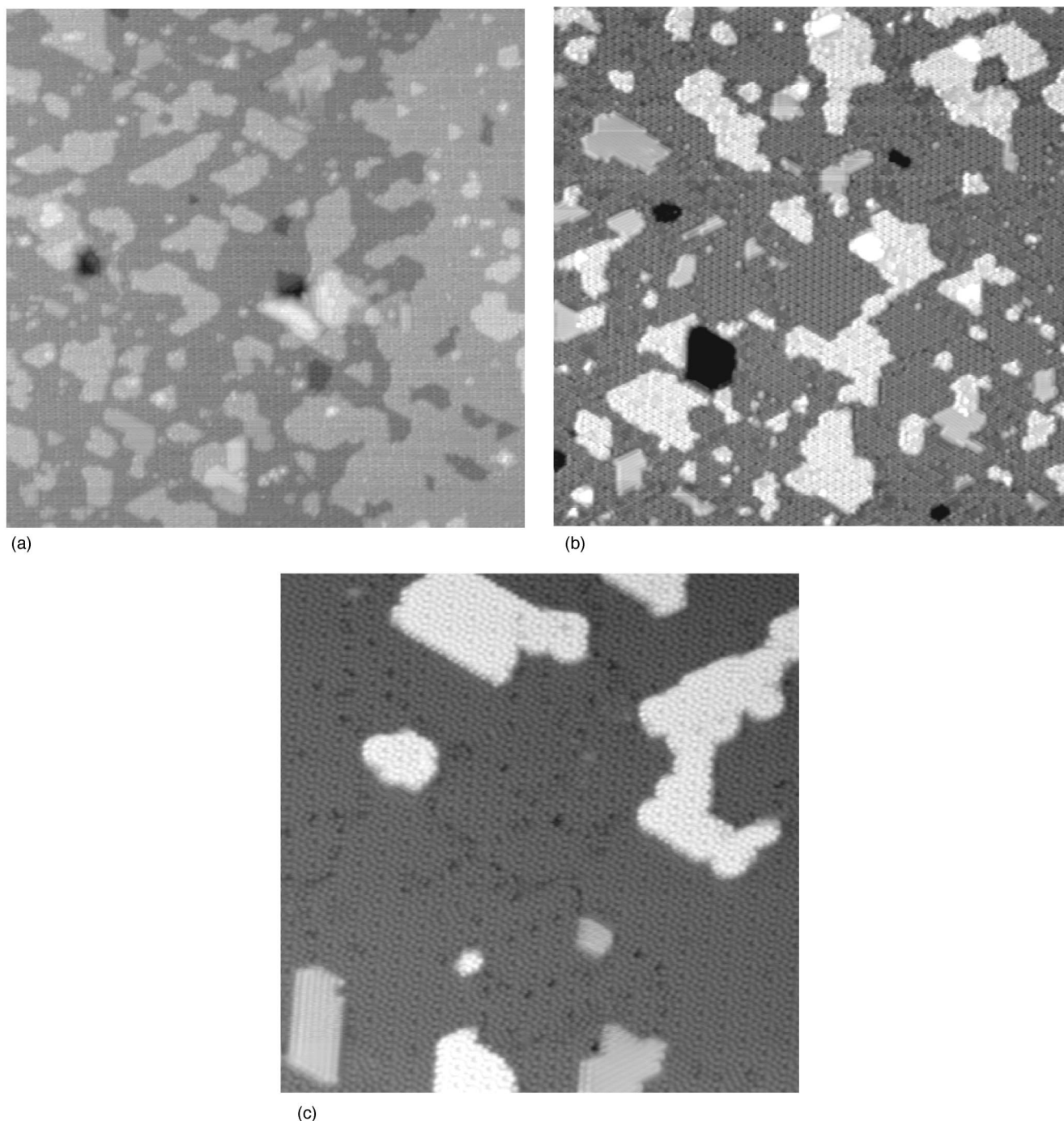


FIG. 3. Higher magnification ( $1000 \times 1000 \text{ \AA}$ ) STM images of the same surfaces imaged in Fig. 2, following growth of (a) 52 BL of Si at  $T = 280^\circ \text{C}$  and 30 BL of Si at (b)  $T = 320^\circ \text{C}$ , (c)  $T = 360^\circ \text{C}$  ( $500 \times 500 \text{ \AA}$  image).

Fig. 8, which form due to nucleation at domain boundaries.<sup>25</sup> The evolution of the pyramids with deposition time at a given temperature seems to primarily consist of the growth of a roughly fixed number of pyramids, as suggested by the numbers shown in Table I, rather than a continual nucleation of new pyramids. This conclusion is also consistent with the rather uniform distribution of sizes observed in Figs. 6(a) and 6(b). However, since the pyramids were identified using parameters determined from the most readily observed structures, it is possible that the continuing (but slow) evolution of new pyramid nuclei [the structures of Figs. 8(a) and 8(b)

may be such a nucleus] is not represented in the tabulated data.

In addition, we do not see any evidence of coalescence of the mounds as they get larger. As the nucleation tends to occur near antiphase boundaries, after longer growth times coalescence may occur along the boundaries, or even later, throughout the surface. But at the temperature range and film thicknesses we are considering, diffusion appears to make these processes difficult and lead to relatively isolated pyramids. Thus, our observation of the pyramidal structures and their evolution during growth appears unrelated (or, at least



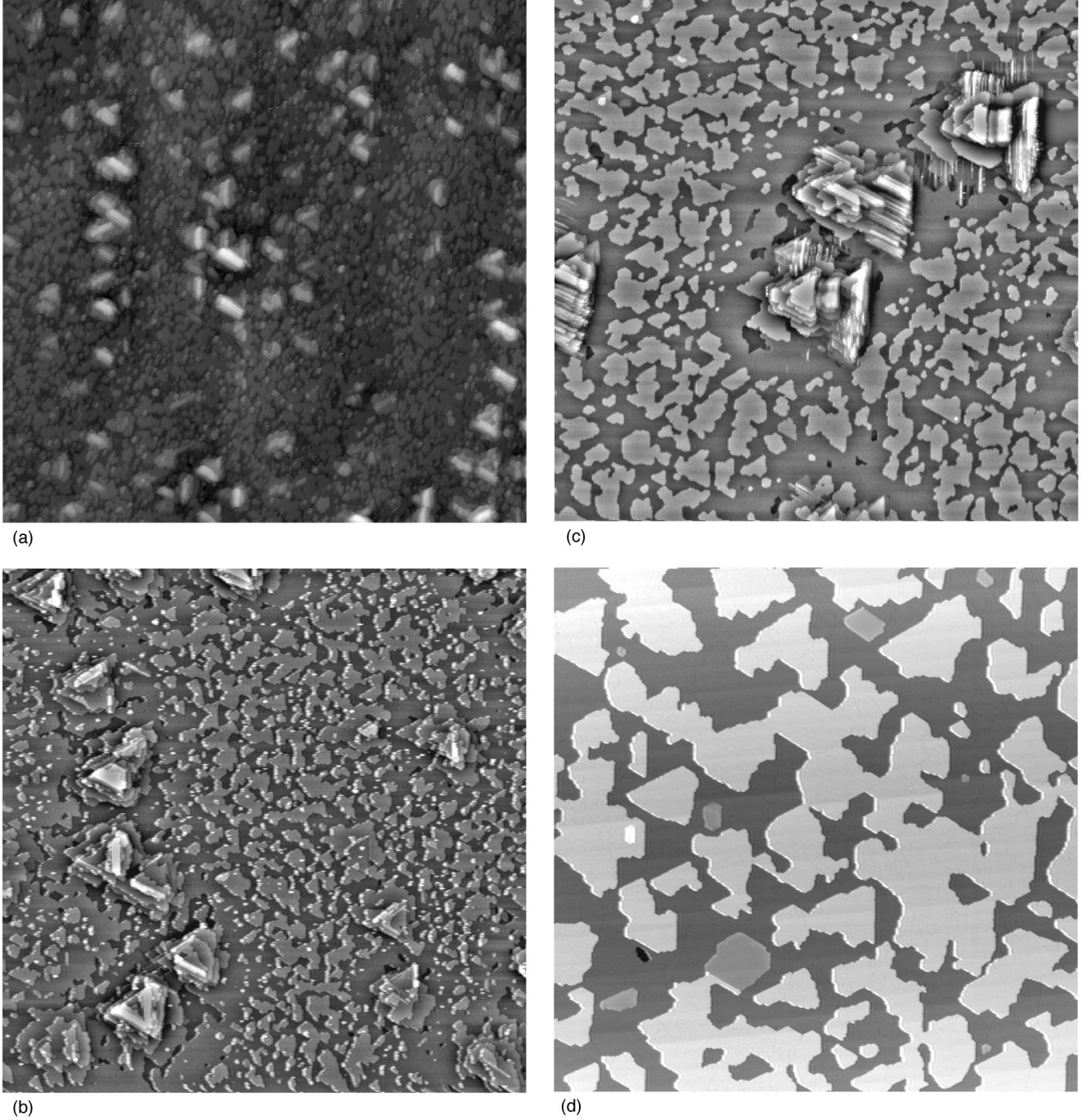


FIG. 4. 5000×5000 Å STM images following deposition (a) of 105 BL of Si at 280 °C [there is a doubled tip, with a tip separation of  $\sim 500$  Å (Ref. 43)], and of 210 BL of Si at the temperatures indicated: (b)  $T=320$  °C, (c)  $T=360$  °C, (d)  $T=410$  °C, (e)  $T=410$  °C (1000×1000 Å).

not related in an obvious manner) to the nonequilibrium coarsening phenomenon associated with the Ehrlich-Schwoebel barrier.<sup>7,10,11,16–18</sup>

### B. Quantitative and scaling analysis

Given the unusual growth characteristics shown in the STM images, it seems unlikely that the standard dynamic scaling predictions of scale-invariant growth should be applicable to our results. To confirm this, we have calculated the width (i.e., the root-mean-square height fluctuations)

$$W(R,t) = \left\langle \sum_{|x| \leq R} [h(\vec{x},t) - \bar{h}(t)]^2 \right\rangle^{1/2} \quad (2)$$

and the equal-time height-height correlation function

$$G(\vec{x},t) = \left( \sum_y [h(\vec{x} + \vec{y},t) - h(\vec{y},t)]^2 \right)^{1/2} \quad (3)$$

of each interface from its STM image. In Eq. (2), the length  $R$  defines the surface patch of size  $R \times R$  over which the



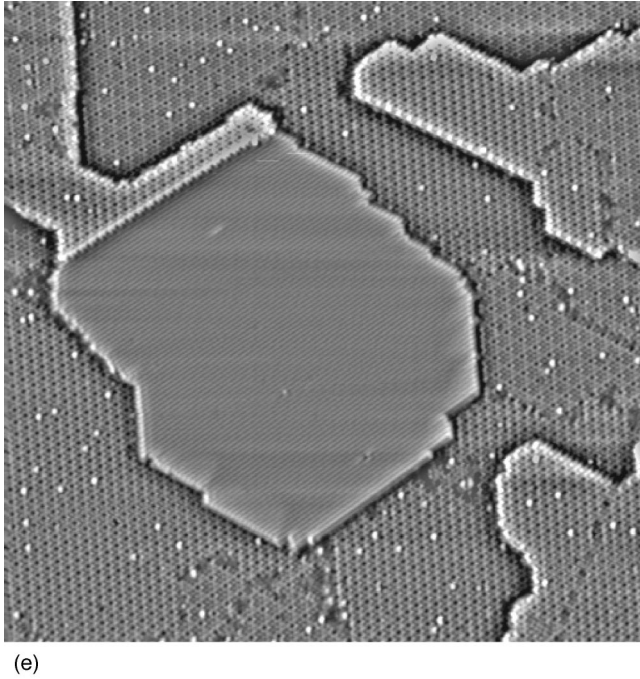
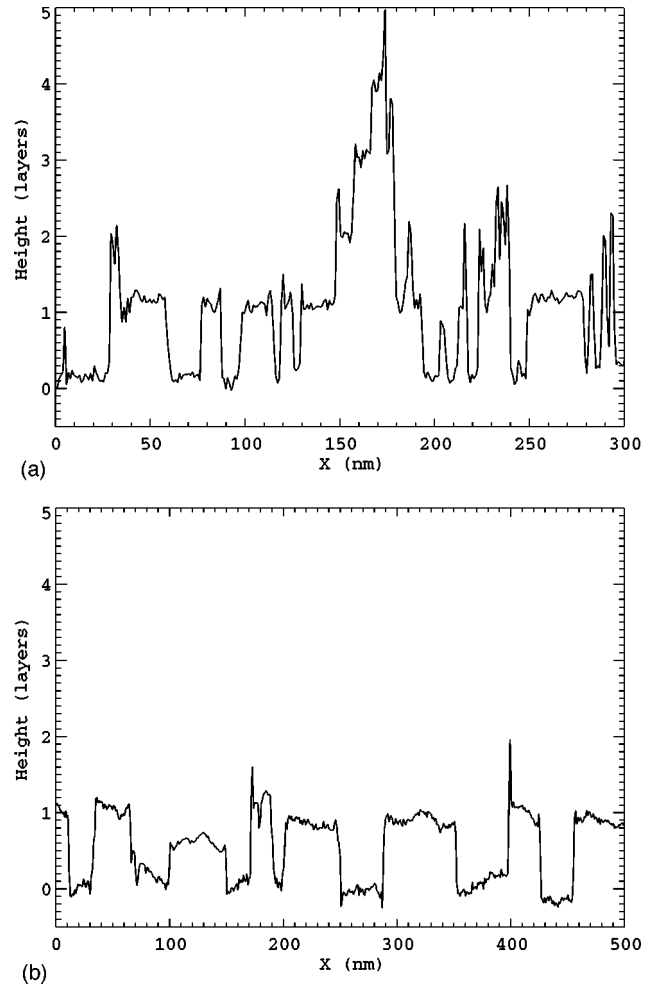


FIG. 4. (Continued.)

width is calculated,  $\bar{h}(t)$  is the mean height of that surface patch, and the brackets indicate an average over all such patches. While the results given are for individual STM images, the values of  $W$  and the plots of  $G(x)$  shown herein do not vary appreciably on different patches of surface. Our general conclusions regarding the presence of dynamical scaling and the morphological characteristics of the grown films presented are fully consistent with all of our data.

Figure 9 shows the correlation function calculated after 52 and 105 BL of growth at  $T=280^\circ\text{C}$  [see Figs. 2(a) and 4(a) (Ref. 43)]. We observe that  $G$  saturates to a value  $G_{\text{sat}}$  as  $x$  becomes large, with the value of  $G_{\text{sat}}$  increasing in time. The correlation length, which we define as the distance  $x$  at which  $G(x,t)$  first saturates, also rises in keeping with the general expectation that at later times lateral dynamical correlations have spread over larger distances:  $\xi_{105}=160\pm 20\text{ \AA}$  while  $\xi_{52}=70\pm 10\text{ \AA}$ . However, Fig. 9 does not manifest linear behavior in  $|\bar{x}|$  (as required by dynamic scaling) over a satisfactorily wide range of lengths to permit the extraction of a meaningful scaling exponent  $\alpha$ . At best, the 105 BL films in Fig. 9 could be interpreted in terms of two different regimes, with an *effective* roughness exponent  $\alpha_{\text{eff}}=0.7\pm 0.1$  in the initial regime ( $x=10\text{--}30\text{ \AA}$ ) crossing over to an *effective* roughness exponent of  $\alpha_{\text{eff}}=0.45\pm 0.05$  ( $x=50\text{--}100\text{ \AA}$ ) prior to the saturation of  $G(x)$ .<sup>43</sup> These effective exponents are quoted merely as a convenient measure of the correlations in the evolving interface and not as true or asymptotic scaling exponents. The data for 52 BL, the upper curve in Fig. 9, saturate far too quickly for us to extract any value for  $\alpha_{\text{eff}}$ . Indeed, the need for multiple decades of linear behavior to observe scaling in experimental situations have been recently emphasized.<sup>53</sup>

The correlation lengths and widths determined from our images are compiled in Table III, and we collect the extracted effective exponents in Table IV. Note that for all  $x < \xi$  in our experiments, we do not find a large effective

FIG. 5. Sample line scans from STM images of Fig. 4 after 210 BL of growth at (a)  $T=320^\circ\text{C}$  and (b)  $T=410^\circ\text{C}$ .

roughening exponent near unity as might be expected for growth in the presence of a mounding instability,<sup>13,17,33</sup> and rather small values for the surface roughness  $W$ . The criteria on  $W$  and  $\xi$  for scale invariant kinetic roughening described in Sec. I are not satisfied in our data. However, our results may not be inconsistent with Yang, Wang, and Lu,<sup>13</sup> who found  $\alpha=1$  and strong kinetic roughening of Si(111) at  $T=275^\circ\text{C}$ , as our experiments were performed at somewhat higher temperatures (see temperature calibration discussion above and below).

The analysis of the interface width as a function of image area provides results similar to those obtained from the correlation function, as shown in Fig. 10. The saturation width is measured to be less than a single-layer height:  $W=0.77c$ ,<sup>43</sup> with  $c$  the height of the  $7\times 7$  unit cell. Again, one finds a ‘‘crossover’’ in the effective exponents extracted from Fig. 10, ranging from  $\alpha_{\text{eff}}=0.78$  to 0.46, and this transition is consistent with the nonlinearity observed in Fig. 9.

There are two reasons why one cannot interpret these images in terms of scale invariance and dynamic scaling. First, the small correlation length ( $\leq 100\text{ \AA}$ ) is an upper limit on the length scale  $x < \xi$  in which scaling can be observed. Hence, crossover effects associated with the saturation of  $G(x)$  obscure the extraction of a reliable scaling exponent  $\alpha$ . At longer times this problem mitigates because  $\xi \sim t^{1/2}$ , but for typical values of  $z=2\text{--}4$  this is a rather slow increase in  $\xi$ . More importantly, the basic  $7\times 7$  unit cell of the Si(111)

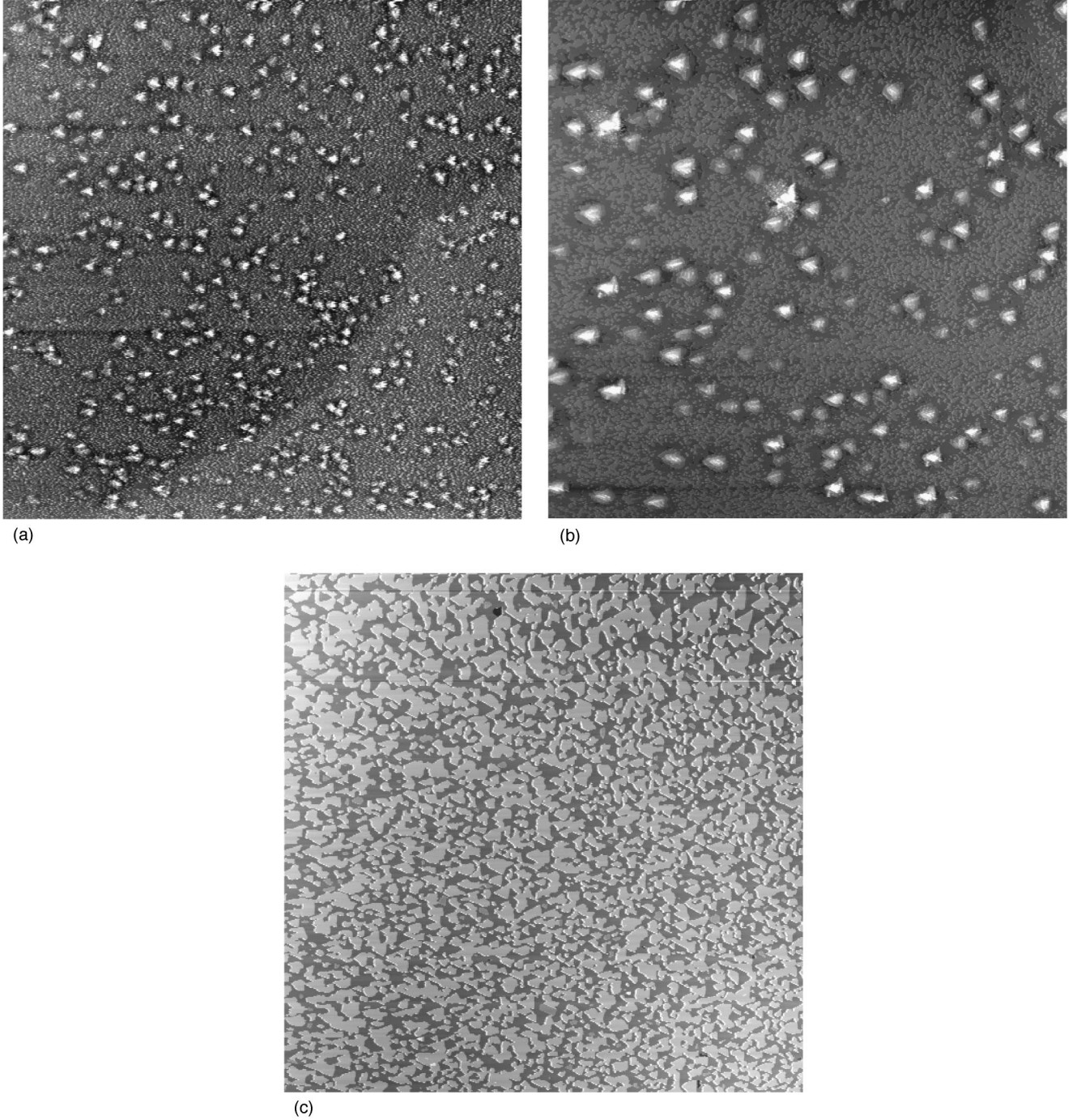


FIG. 6.  $2\ \mu\text{m} \times 2\ \mu\text{m}$  STM images measured after 210 BL of deposition at the indicated temperatures. (a)  $T = 320\ ^\circ\text{C}$ , (b)  $T = 360\ ^\circ\text{C}$ , (c)  $T = 410\ ^\circ\text{C}$ .

surface itself has lateral dimensions of  $a \approx 30\ \text{\AA}$ , and measuring correlations below this scale is essentially meaningless. To demonstrate the importance of this, the inset of Fig. 9 (52 BL for a  $100 \times 100\ \text{nm}^2$  STM image at  $T = 280\ ^\circ\text{C}$ ) seems to display compelling dynamic scaling behavior due to the linearity of  $G(x)$  over  $x = 2 - 30\ \text{\AA}$ , with  $\alpha_{\text{eff}} \approx 0.5$ . However such a measurement has dubious relevance to the large-scale surface roughness because the entire “scaling” regime here corresponds to  $x \leq a$ : one is essentially probing the roughness of the  $7 \times 7$  unit cell. Therefore no particular significance can be attached to this effective exponent even

though the linear fit is quite good. In general, as is known theoretically, the regime over which we can detect scaling has intrinsic lower and upper limits: we can at best probe scaling for  $a < x < \xi(t)$ . The results at  $T = 280\ ^\circ\text{C}$  point out that the numerical values of effective “exponents” can be deceptive and readily influenced by a variety of nonscaling effects.

A naive calculation of the exponent  $\beta_{\text{eff}}$  from the dynamical scaling relation  $W \sim t^\beta$  for the two data points at  $T = 280\ ^\circ\text{C}$  gives an order of magnitude estimate  $\beta_{\text{eff}} = 0.24 \pm 0.05$  (statistically consistent with  $\beta_{\text{eff}} = 0.31 \pm 0.05$  esti-

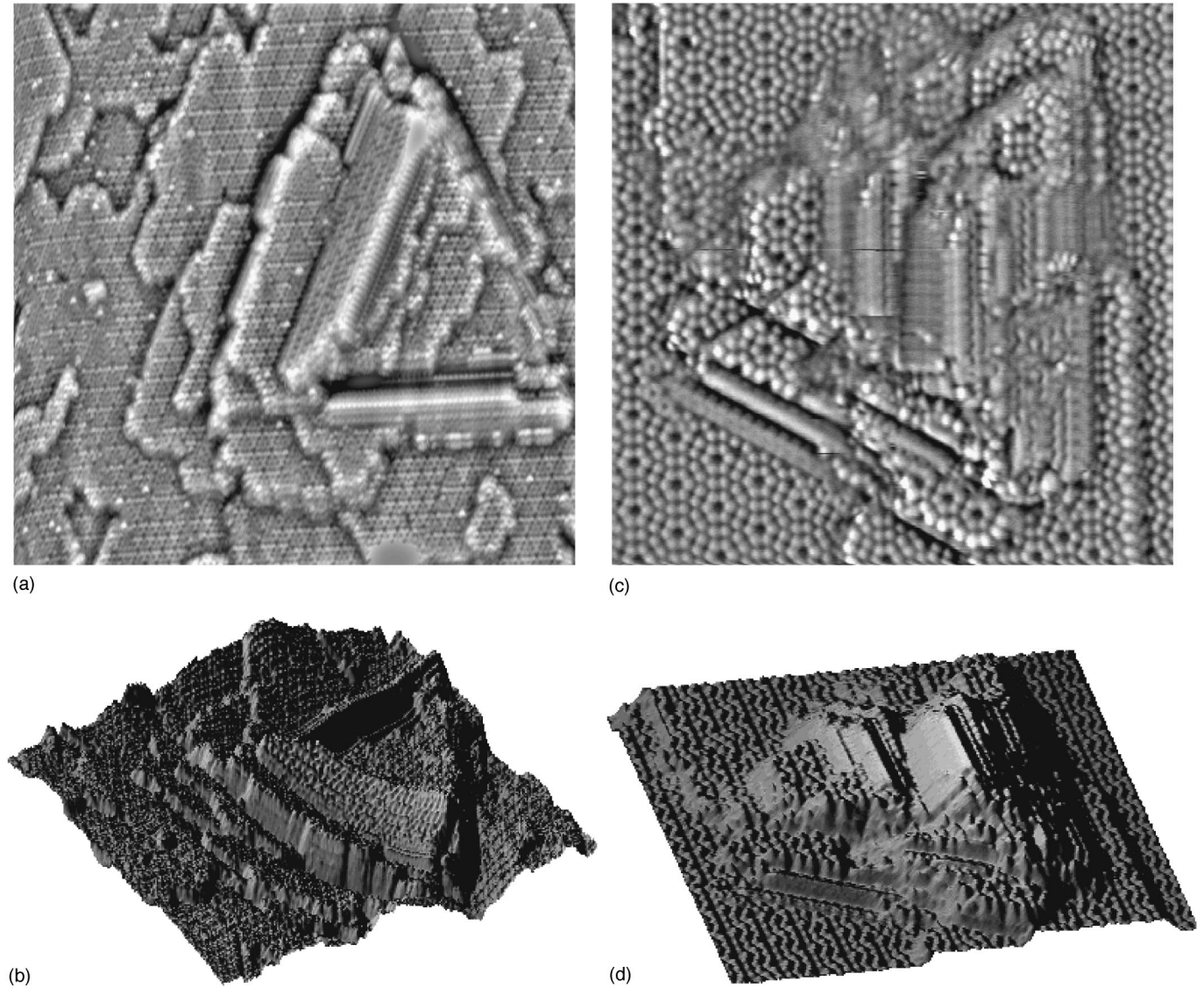


FIG. 7. STM images of the pyramidal structures shown in a filtered format to emphasize the atomic ordering, and in a 3D shadowed format to emphasize their height variation. (a)  $600 \times 600$  Å filtered image after 210 BL growth at  $T = 320$  °C, (b) same image shown in shadowed format. (c)  $300 \times 300$  Å filtered format image after 67 BL growth at  $T = 360$  °C, (d) same image shown in shadowed format.

mated from the saturated value of the correlation function,  $G_{\text{sat}} \sim t^\beta$ ). While comparable in magnitude to some of the fourth-order nonlinear continuum theories of kinetic roughening,<sup>4</sup> this limited data set does not allow for a dynamic scaling interpretation for reasons discussed above.

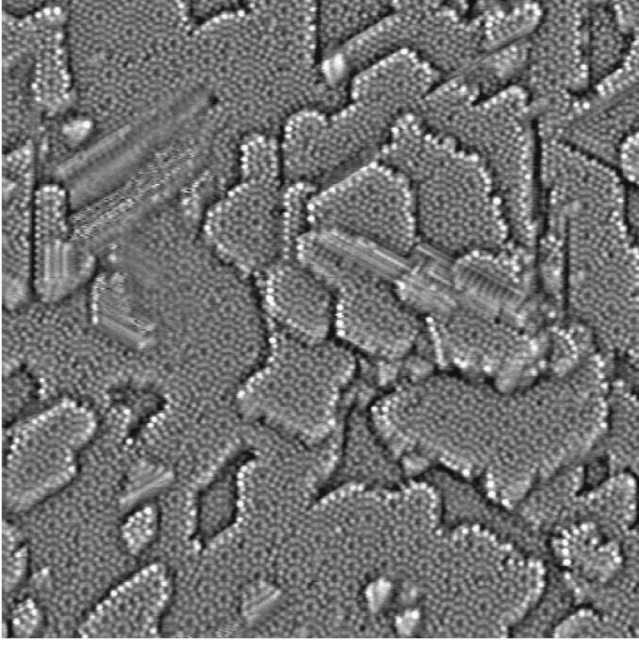
For growth of a 105 BL film at  $T = 320$  °C, we find that  $W = 0.73c$  and from  $G(x)$  in Fig. 11 we measure  $\xi_{105} \sim 180 \pm 20$  Å. Again, as  $\xi_{105} \sim 6a$  is relatively small,  $G(x)$  provides only a qualitative estimate of the growth of correlations, and not a value meaningful in the context of the kinetic roughening theory. Nevertheless, rotely calculating the effective roughness exponent on  $[a, 5a]$  gives a value  $\alpha_{\text{eff}} = 0.32 \pm 0.05$ , much less than unity for  $x \leq \xi$ .

The correlation function after 210 BL of growth at  $T = 320$  °C (Fig. 11) exhibits a small but roughly linear region over  $x = [a, \xi_{210} \sim 10a]$ , yielding  $\alpha_{\text{eff}} = 0.29 \pm 0.03$ . The surface width has grown to  $W = 0.97c$ , giving the naive estimate of  $\beta_{\text{eff}} = 0.40 \pm 0.05$  (from  $G_{\text{sat}}$ , we estimate  $\beta_{\text{eff}} = 0.48 \pm 0.05$ ). Once more, we emphasize that although such

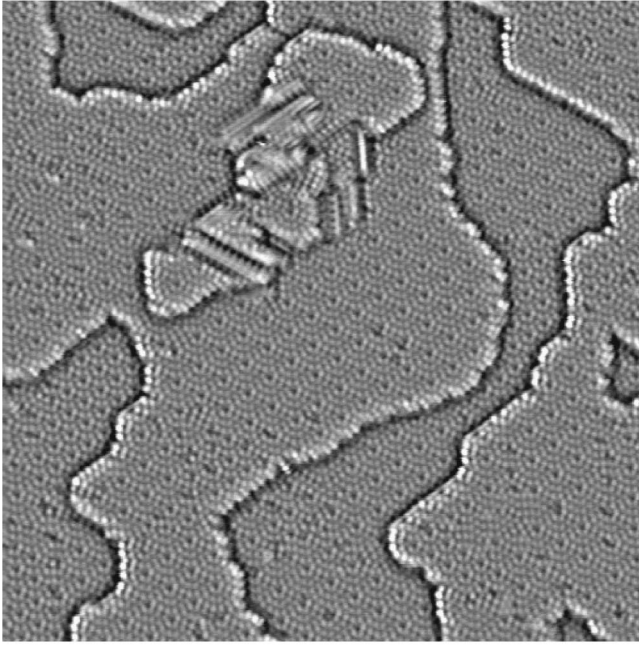
a large  $\beta_{\text{eff}}$  qualitatively indicates a rapid growth in  $W$ , the actual surface roughness is still rather small ( $W \approx c$ ), and dynamic scaling of  $W$  with time is not confirmed by these data although  $W$  and  $\xi$  are at the threshold where we expect it to become observable.

An analysis of the 210 BL thick film grown at  $T = 360$  °C yields similar results, as shown in the inset of Fig. 11. The correlation length is approximately  $500 \pm 50$  Å, and we compute an effective exponent of  $\alpha_{\text{eff}} = 0.65 \pm 0.10$  for  $x = 10 - 40$  Å which changes to  $\alpha_{\text{eff}} = 0.36 \pm 0.05$  for  $x = 50 - 500$  Å. A rapid rise in the surface width ( $\beta_{\text{eff}} = 0.70 \pm 0.10$ ) correlates directly with the growth of the isolated pyramidal features.

We have calculated the diffraction profiles for our STM images, as described above. The calculated profiles are noisy, presumably due to statistical averaging limitations even for our largest ( $2\text{-}\mu\text{m}$ ) images. However, convolution with a narrow instrumental response function yields profiles narrower but comparable in width (see FWHM in Table III)



(a)



(b)

FIG. 8. STM images showing regions of complex reconstruction and multilayer growth. These filtered images are  $600 \times 600 \text{ \AA}^2$  (a) 20 BL growth at  $T=360 \text{ }^\circ\text{C}$ ; (b) 67 BL of growth at  $T=360 \text{ }^\circ\text{C}$ .

to those previously measured for the nonscaling growth of Si/Si(111) at  $350 \text{ }^\circ\text{C}$ .<sup>13</sup> These calculations are further evidence that kinetic roughening in the Si/Si(111) system appears to occur within a relatively narrow window of temperature. The thickest films grown at  $T=320 \text{ }^\circ\text{C}$  and  $360 \text{ }^\circ\text{C}$  also yielded slightly asymmetric diffraction profiles. The asymmetry varied with the perpendicular wave-vector transfer, suggesting that it arises from scattering from planes tilted from the (111) surface by roughly  $20\text{--}30$  degrees for  $T=275 \text{ }^\circ\text{C}$ ,<sup>33</sup> and thus may be the result of scattering from the pyramid structures. Interestingly, a naive computation of the

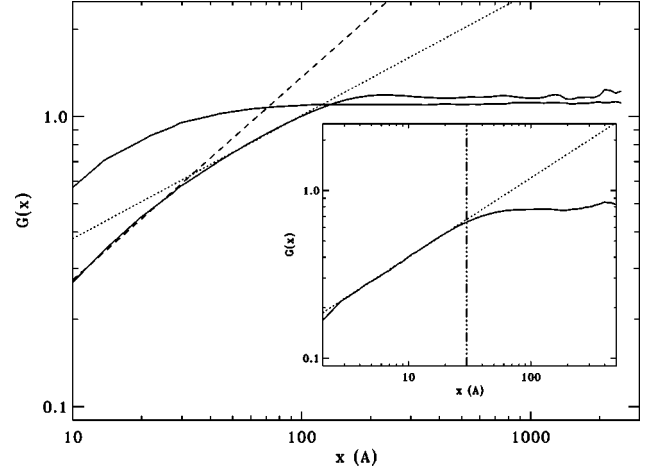


FIG. 9. Correlation function,  $G(x)$ , calculated from  $5000 \times 5000 \text{ \AA}^2$  STM images of surfaces following 52 and 105 BL (Ref. 43) of growth at  $T=280 \text{ }^\circ\text{C}$  (at large  $x$ , the lower and upper plots, respectively). The lack of a single linear region does not allow for the definition of the scaling exponent  $\alpha$ : for 105 BL, the best fit lines shown give  $\alpha_{\text{eff}}=0.45 \pm 0.05$  ( $x=50\text{--}100 \text{ \AA}$ ) and  $\alpha_{\text{eff}}=0.69 \pm 0.10$  ( $x=10\text{--}30 \text{ \AA}$ ). Inset:  $G(x)$  vs  $x$  for a  $1000 \times 1000 \text{ \AA}^2$  image following 52 BL of growth at  $T=280 \text{ }^\circ\text{C}$ . Note that the linear regime ( $\alpha_{\text{eff}} \sim 0.5$ ) physically corresponds to distances  $x \leq a$ , where  $a=30 \text{ \AA}$  is the  $7 \times 7$  unit-cell dimension.

average angle made by the pyramid sides with the Si(111) surface from the data in Table II shows that our  $T=280 \text{ }^\circ\text{C}$  data falls in this range, and that the angle drops with  $T$ . However, the variability of pyramid shapes seen in Fig. 7 (and indeed, the variation in the slope on different sides of the same pyramid) does not allow for a good quantitative comparison.

#### IV. DISCUSSION

Our study of growth in the Si/Si(111) system indicates dramatic changes in the nature of growth over a narrow temperature range, with the length scale for island formation decreasing from approximately  $500 \text{ \AA}$  at  $360 \text{ }^\circ\text{C}$  to approximately  $160 \text{ \AA}$  at  $280 \text{ }^\circ\text{C}$ . This decrease in diffusion length is qualitatively consistent with previous LEED observations in which  $\xi$  fell in passing from perfect layer-by-layer growth at  $350 \text{ }^\circ\text{C}$ , to rough growth manifesting dynamic scaling and the loss of overlayer order (e.g., disappearance of intensity in the  $7 \times 7$  beams) at  $275 \text{ }^\circ\text{C}$ .<sup>13</sup> However, our additional STM measurements have detected the formation of pyramidal structures upon extensive deposition down to temperatures roughly  $10\text{--}20 \text{ }^\circ\text{C}$  above their rough growth regime. This is quite different from the morphological changes expected in passing from kinetically rough scale invariant growth to layer-by-layer growth. Scale invariant growth should demonstrate a much more uniform distribution of feature sizes than we observe. We first discuss the physical nature of the observed growth in light of previous observations, and then theoretical issues pertaining to modeling such a mechanism.

At elevated temperatures where the diffusion length far exceeds typical terrace sizes, growth of Si on Si(111) proceeds via a layer-by-layer growth mode.<sup>44</sup> This mechanism dominates down to about  $700 \text{ }^\circ\text{C}$ , at which point nucleation

TABLE III. Measured surface width  $W$ , correlation length  $\xi$ , and the FWHM of the calculated intensity profile for  $500 \times 500 \text{ nm}^2$  images. The width is given in terms of the height of the  $7 \times 7$  unit cell,  $c$ . Errors in  $W$  and  $\xi$  are  $\sim 10\%$ , and  $\sim 20\%$  for FWHM.

Film thickness	$T = 280^\circ\text{C}$	$T = 320^\circ\text{C}$	$T = 360^\circ\text{C}$	$T = 410^\circ\text{C}$
30 BL	No data	$W = 0.70c$ $\xi = 60 \text{ \AA}$ FWHM = $0.015 \text{ \AA}^{-1}$	$W = 0.40c$ $\xi = 130 \text{ \AA}$ FWHM = $0.015 \text{ \AA}^{-1}$	$W = 0.38c$ $\xi = 220 \text{ \AA}$ FWHM = $0.015 \text{ \AA}^{-1}$
52 BL ( $T = 280^\circ\text{C}$ )	$W = 0.65c$ $\xi = 70 \text{ \AA}$	No data	$W = 0.37c$ $\xi = 270 \text{ \AA}$ FWHM = $0.015 \text{ \AA}^{-1}$	No data
67 BL ( $T = 360^\circ\text{C}$ )	FWHM = $0.015 \text{ \AA}^{-1}$			
105 BL	<sup>a</sup> $W = 0.77c$ $\xi = 160 \text{ \AA}$ FWHM = $0.016 \text{ \AA}^{-1}$	$W = 0.73c$ $\xi = 180 \text{ \AA}$ FWHM = $0.016 \text{ \AA}^{-1}$	No data	No data
210 BL	No data	$W = 0.97c$ $\xi = 300 \text{ \AA}$ FWHM = $0.026 \text{ \AA}^{-1}$	$W = 0.95c$ $\xi = 500 \text{ \AA}$ FWHM = $0.037 \text{ \AA}^{-1}$	$W = 0.50c$ $\xi = 250 \text{ \AA}$ FWHM = $0.020 \text{ \AA}^{-1}$

<sup>a</sup>Double tip effect should be small (Ref. 43).

and growth of islands becomes a competing process.<sup>45,46</sup> Homogeneous nucleation of islands which form in the  $7 \times 7$  structure has been observed down to at least  $350^\circ\text{C}$ .<sup>28,34,47</sup> Simultaneous nucleation of islands of metastable structures such as the  $5 \times 5$  has also been extensively reported.<sup>29,42,46,48</sup>

In addition, heterogeneous nucleation, in which Si islands nucleate preferentially at antiphase domains in the  $7 \times 7$  structure, occurs as a competing process to homogeneous nucleation.<sup>25,30,34</sup> A detailed analysis of the islands that form during heterogeneous nucleation has shown that about two-thirds of the time they form in metastable reconstructions, such as the  $5 \times 5$  and  $2 \times 1$  reconstruction.<sup>25</sup> Continuing growth on top of these islands often occurs in the form of metastable structures, consistent with LEED observations of the formation of mixed  $5 \times 5$  and  $7 \times 7$  periodicity during the growth of thick layers of Si/Si(111).<sup>29</sup>

We have shown here that the process of nucleation of

metastable structures at domain boundaries remains important following tens of layers of growth, as shown in Fig. 3. It seems very likely that these metastable structures are the nuclei for the formation of small multilayer structures, such as those shown in Figs. 8(a) and 8(b), and that these are in turn the origin of the pyramidal structures observed in still thicker layers [e.g., Figs. 4(a)–4(c), 6(a), 6(b), and 7]. We postulate that the formation and growth of these structures is the result of a sort of kinetic instability in which preferential formation of new defect structures at the original antiphase domain boundaries causes runaway growth of the metastable pyramidal structures. For this to occur, the defect structures created in each stage of the process would need to be preferential binding sites for incoming Si atoms. This is certainly a property of the observed pyramids, as shown by the presence of a “denuded zone” around the pyramids in Figs. 4(a)–4(c). It is clear that Si atoms deposited within a diffu-

TABLE IV. Effective “exponents” for  $500 \times 500 \text{ nm}^2$  STM images. The upper value of  $\alpha_{\text{eff}}$  is measured on length scales near the saturation of  $G(x)$ , while the lower value (when present) is extracted from the small- $x$ , nonscaling region near  $x = a$ ; note that this latter value tends to be numerically greater. Values of  $\beta$  come from the increase in  $W$  with time.  $N/M$  = not measurable. The presence of scale-invariant growth is generally not well supported; see text.

Film thickness	$T = 280^\circ\text{C}$	$T = 320^\circ\text{C}$	$T = 360^\circ\text{C}$	$T = 410^\circ\text{C}$
30 BL	No data	$\alpha_{\text{eff}}: N/M$	$\alpha_{\text{eff}}: N/M$	$\alpha_{\text{eff}} = 0.47(5)$
52 BL ( $T = 280^\circ\text{C}$ )	$\alpha_{\text{eff}}: N/M$	No data	$\alpha_{\text{eff}} = 0.36(5)$	No data
67 BL ( $T = 360^\circ\text{C}$ )	[ $\alpha_{\text{eff}} = 0.50(2)$ ]			
105 BL	<sup>a</sup> $\alpha_{\text{eff}} = 0.45(5)$ [ $\alpha_{\text{eff}} = 0.7(1)$ ]	$\alpha_{\text{eff}} = 0.32(5)$	No data	No data
210 BL	No data	$\alpha_{\text{eff}} = 0.29(3)$ [ $\alpha_{\text{eff}} = 0.6(1)$ ]	$\alpha_{\text{eff}} = 0.36(5)$ [ $\alpha_{\text{eff}} = 0.65(10)$ ]	$\alpha_{\text{eff}} = 0.43(5)$
$\beta_{\text{eff}}$	0.24-0.31	0.40-0.48	0.67-0.77	0-0.13

<sup>a</sup>Double tip effect should be small (Ref. 43).

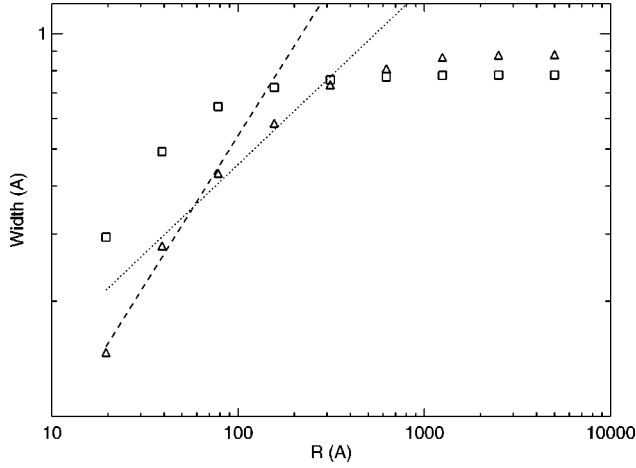


FIG. 10. Plot of the width  $W(R)$  vs  $R$ , the patch size over which  $W$  is computed, for  $T=280^\circ\text{C}$  for 52 BL ( $\square$ ) and 105 BL ( $\triangle$ ) of growth. Fitting to the 40–320 Å region for 105 BL gives  $\alpha_{\text{eff}}=0.46$  (small dashes), while  $\alpha_{\text{eff}}=0.78$  from 20–80 Å (long dashes). Compare with Fig. 9 above.

sion length of the growing pyramids have preferentially attached to (and seemingly have ascended) the pyramids rather than remaining free to coalesce into two-dimensional islands.

Other possible explanations for the formation of the pyramid structures, which we reject, are mound formation due to an Ehrlich-Schwoebel barrier<sup>14,15</sup> or impurity pinning. In the case of an Ehrlich-Schwoebel barrier, strong three-dimensional growth is expected at the earliest stages of growth because atoms that are deposited on top of existing islands do not cross the island edges easily, and thus nucleate to form new islands on top of the old. This process leads to a characteristic “wedding cake” structure in growth<sup>49</sup> or to large-scale mound formation<sup>10–12</sup> followed by coarsening. Any stepped structures on Si should be subject to these barriers, and not just those near domain boundaries. Our observation of relatively flat growth over the majority of the sur-

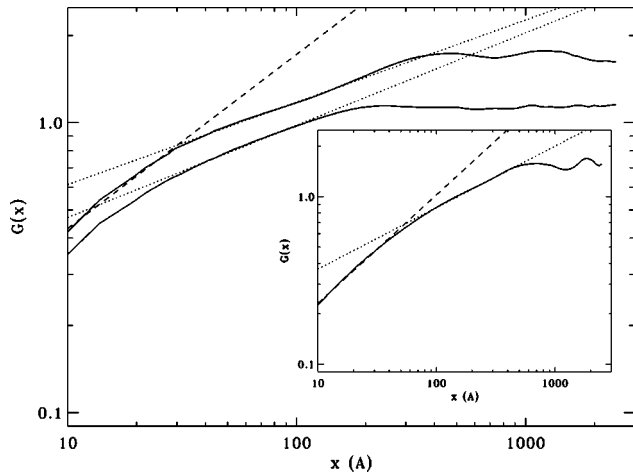


FIG. 11.  $G(x)$  for  $5000 \times 5000 \text{ Å}^2$  STM images at  $T=320^\circ\text{C}$ . After 105 BL (bottom), we find  $\alpha_{\text{eff}}=0.32 \pm 0.05$  for  $[a, 5a]$ . After 210 BL of growth (top)  $\alpha_{\text{eff}}=0.29 \pm 0.03$  on  $[a, 10a]$ . For  $x \leq a$  at 210 BL,  $\alpha_{\text{eff}}=0.6 \pm 0.1$ . Inset:  $G(x)$  for a  $5000 \times 5000 \text{ Å}^2$  STM image after growth of 210 BL at  $T=360^\circ\text{C}$ . The best fit was for  $[2a, 17a]$ , for which  $\alpha_{\text{eff}}=0.36 \pm 0.05$ ; the fit for  $x=10-40 \text{ Å}$  gave  $\alpha_{\text{eff}}=0.65 \pm 0.10$ .

face area (see Tables I and II) is not consistent with a simple Ehrlich-Schwoebel mechanism. Furthermore, the complex structures of the pyramids that we observe, such as that in Fig. 7, where there is a deep pit in the center of the pyramid and the walls seem to join together is also not consistent with a simple mechanism of preferential nucleation of islands on top of islands. Our observed pyramids, then, are not mounds or wedding cake structures.

It is of course difficult to absolutely rule out the possibility of impurities playing a role in forming these pyramid structures. Indirect evidence against this possibility is the observation of Yang, Wang, and Lu<sup>33</sup> of the formation of very large well oriented facets following growth on an intentionally roughened surface. It seems reasonable that these observed facets are much larger and better ordered versions of the pyramids that we have observed. This result strongly suggests that it is the characteristics of the surface order, rather than impurities, that govern the nucleation of the structures. Carbon is not likely to be the origin of the pyramids, since the surfaces can be flashed clean following growth without the formation of the characteristic step pinning and ultimate faceting that occurs in the presence of carbon.<sup>50–52</sup> We cannot rule out the effect of other impurities, such as hydrogen, on the basis of any direct observation. However, the consistency of the observations of crystalline structures similar to the metastable reconstructions of Si(111) over the full range of growth temperatures and conditions provides strong indirect evidence that the pyramid formation is an intrinsic property of Si growth on Si(111), and is not extrinsically caused by surface impurities.

Next, we consider these STM images from the point of view of kinetic roughening theory and scale invariance. For reference, we recall that prior HRLEED experiments on Si/Si(111)<sup>13</sup> at  $T=275^\circ\text{C}$  found that  $W=1.9c$  and FWHM  $\sim 0.22 \text{ Å}^{-1}$  after 70 BL of growth, increasing to  $W=2.8c$  and FWHM  $\sim 0.27 \text{ Å}^{-1}$  after deposition of 130 BL. At  $T=275^\circ\text{C}$ , scaling according to the noisy Herring-Mullins equation was detected with  $\alpha=1$ ,<sup>13</sup> a value for which formation of pyramids with a preferred slope has also been predicted theoretically.<sup>17</sup> At  $T=350^\circ\text{C}$ , flat nonkinetically rough films were found with FWHM  $< 0.03 \text{ Å}^{-1}$  that are likely comparable to the structures we observe at our nominal temperature of  $410^\circ\text{C}$  (Ref. 13) (and perhaps even lower due to the very small FWHM values in Table III). We point out here, however, the considerably greater ability of HRLEED to generate highly statistically averaged diffraction profiles (over a larger total area) as compared to STM experiments. As such, our simulated diffraction profiles are intended to be a qualitative consistency check. Nevertheless, our FWHM values do reflect the basic smoothness of the STM images and that roughness is increasing somewhat with added deposition. Further, they provide us with our best direct comparison with the data in Ref. 13.

We have probed a temperature range between the kinetically rough and layer-by-layer growth regimes. Based on the rough constancy of  $\alpha_{\text{eff}}$  in time at  $T=320^\circ\text{C}$  (Table IV), that  $W \sim c$  and  $\xi \sim 10a$ , and the reasonably linear plot in Fig. 11 at 210 BL for  $x < \xi$ , there is limited evidence to suggest that dynamical scaling may be emergent at  $T=320^\circ\text{C}$  once  $\xi \geq 10a$ . At higher temperatures, as well as for  $T=280^\circ\text{C}$ , scale-invariant growth was not observed. Our best estimate



for the *effective* roughness exponent is  $\alpha_{\text{eff}} \approx 0.3\text{--}0.5$ , which is not consistent with unity and exceeds  $\alpha$  for the known solid-on-solid continuum dynamic growth universality classes for a planar substrate.

Both STM and diffraction experiments seem to imply similarly small correlation lengths:  $\xi < 20a$  for all STM images and  $\xi < 10a$  for the diffraction experiment<sup>13</sup> at  $T = 275^\circ\text{C}$  [where in the  $\alpha = 1$  case, we estimate  $\text{FWHM} = W/\xi$  (Ref. 41)]. Since dynamical scaling is expected only for  $x < \xi$ , sensitivity to finite size effects may account for the large discrepancy in  $\alpha$  between the two experiments. It is also possible, and we feel more likely given the uncertainties in temperature calibration, that our growth temperatures are actually somewhat higher on the temperature scale of Ref. 13 than one would naively expect. This would also explain the lower effective roughness exponent we extract.

Because  $\text{FWHM} \sim W^{1/\alpha}/\xi$  (from the form for  $\eta$  given in Ref. 41), the similarities in  $\xi$  imply that the detected differences in FWHM arise from significant differences in  $W$  for the two experiments. Since a higher temperature is known to reduce the height fluctuations on a growing surface,<sup>19</sup> the lower values of  $W$  in our STM experiment would produce a smaller FWHM. However, we doubt that a mere  $5^\circ\text{C}$  increase in temperature can result in such a drastic difference as finding  $\alpha = 1$  and strong evidence of scaling at  $275^\circ\text{C}$  via HRLEED (Ref. 13) versus our STM observation of (at best)  $\alpha_{\text{eff}} \sim 0.4$  with no dynamic scaling at  $280^\circ\text{C}$ . In our opinion, it appears likely that a systematic offset of about  $+(10\text{--}20)^\circ\text{C}$  should be applied to our temperatures to compare with those of Ref. 13.

Mechanistically, we hypothesize that as  $T$  is lowered below our nominal  $280^\circ\text{C}$ ,  $W$  rises increasingly rapidly due to progressively more robust growth and nucleation of pyramids. A widespread nucleation of pyramids in the diffraction experiments of Ref. 13 would be consistent with a finding of  $\alpha = 1$ .<sup>17</sup> Hence, it seems reasonable to suppose that Yang's surface<sup>13</sup> contained many more coalescing young pyramids, such as in Fig. 8, than appeared in our experiment. Differences in the density of antiphase boundaries may also be an important factor influencing the comparison of these experiments since such boundaries can act as preferred nucleation sites on Si(111).<sup>25,32</sup> Due to these difficulties, it would be desirable to acquire simultaneous diffraction and STM data for the same surface.

## V. CONCLUSIONS

By probing an intermediate temperature regime between the extremes of rough and smooth growth, we have shown that nucleation and growth of metastable structures at domain boundaries plays an important role in the crossover to kinetically rough growth of Si on Si(111) with decreasing temperature. The number density of the resulting pyramid structures increases as the growth temperature is reduced below the threshold for layer-by-layer growth. There is roughening of highly localized areas of the surface resulting in the emergence of pyramidal structures. It is the growth of these isolated objects alone that leads to the observed increase in the global surface roughness with time. However, there is no conclusive evidence for spatial and temporal dynamic scaling in our data, since the correlation length  $\xi < 10a$  and the

width  $W < c$  are simply too small for widespread correlations to be observed. See Ref. 53 for a broad look at the issue of a limited distance range and the implications for dynamical scaling.

Practically speaking, one expects a finite-temperature window in which thick films might eventually yield scale-invariant morphologies. At high temperatures [ $T \geq 410^\circ\text{C}$  here, and  $T \geq 350^\circ\text{C}$  in (Ref. 13)], atoms are so mobile that  $\xi$  is very large and  $W$  remains small and unchanged [Table III and Figs. 2(c) and 4(c)], while at low temperatures prohibitively long times are needed so that  $\xi$  significantly exceeds the  $7 \times 7$  unit cell size.

The roughening that was observed in our experiments is interesting for it is exclusively due to the formation of small areas of tall, pyramidal structures whose number density decreases with increasing temperature (Tables I and II). In principle, the pyramids may be caused by extrinsic effects, but we have argued that this is unlikely. The pyramidal structures are intriguing as they demonstrate a range of surface reconstructions while evolving rapidly during growth. The pyramids tend to be isolated by expanses of flat surface and cover a small fraction of the total surface area. This is likely due to our elevated growth temperatures (as compared with Ref. 13) and the preferential nucleation of structures at antiphase boundaries.<sup>25</sup> In HRLEED experiments<sup>13</sup> at temperatures slightly lower than ours, we posit that these pyramids have become widespread on the surface resulting in considerable roughness and detectable dynamic scaling behavior.

Based on visible denuded zones around the pyramids we conclude that they draw in atoms from a relatively smooth two- or three-layered surrounding surface. The smooth regions comprise  $\sim 90\%$  or more of the surface and grow in a layer-by-layer fashion without demonstrating the local kinetic instability manifested by the pyramids. Interestingly, then, the surface exhibits two different growth modes simultaneously: localized unstable pyramid formation occurs at antiphase boundaries within a background of layer-by-layer growth away from the pyramids.

The images presented here do not generally support scale-invariant kinetic roughening due to small correlation lengths  $\xi$  on the scale of the  $7 \times 7$  reconstruction size  $a$ . Comparing our results with the diffraction experiment,<sup>13</sup> it seems there is also a required minimum height fluctuation amplitude  $W$  in order to encourage widespread growth. While not measured directly, we argue that one should minimally require  $W > c$ . At later times one might detect a scale-invariant morphology, but our results suggest continued increase in the size of the pyramids without significant coalescence even for our lowest measured temperature, nominally  $T = 280^\circ\text{C}$ . We suspect the scaling seen at  $T = 275^\circ\text{C}$  for Si/Si(111) in Ref. 13 results from a situation in which widespread pyramid coalescence did occur, and that their quoted temperature is  $10\text{--}20^\circ\text{C}$  lower on our temperature scale. Hence, the emergence of dynamic scaling in the Si/Si(111) system may be quite sensitive to relatively small temperature differences and to details of substrate preparation (i.e., density of antiphase boundaries).

Any traces of kinetic roughening may simply be due to well-known islanding processes in the flat regions convolved with the occasional emergence of localized rapidly growing structures. The fact that  $W < c$  makes this a reasonable sup-

position, and the majority of the increase in  $W$  with time is found to be due to the evolution of the individual pyramids. The STM images also show that these pyramids possess a well-defined characteristic size. That observation is patently inconsistent with the concept of a *scale-invariant* surface for which structures on all scales should be simultaneously present. In fact, our finding of the simultaneous presence of two distinct growth modes is explicit evidence against scale-invariant growth over the time and length scales of our observation.

This systematic STM study of Si/Si(111) growth suggests that the emergence of scale-invariant kinetic roughening can require a rather subtle understanding of detailed growth processes (e.g., pyramid formation) and the applicable atomistic length scales (e.g., the  $7 \times 7$  unit-cell size). A brute force

implementation of dynamic scaling machinery to an arbitrary growth problem may lead to extraction of effective dynamical critical exponents,<sup>53</sup> which may not necessarily be meaningful with respect to the common continuum growth theories. Specifically, and as suggested by Figs. 9 and 11 and Table IV, crossover effects induced by various length scales associated with stable and metastable surface structures and reconstructions during kinetically rough real growth may be important.

## ACKNOWLEDGMENTS

This work has been supported by the US-ONR and the NSF-MRSEC at the University of Maryland.

- 
- <sup>1</sup>M. Kardar, G. Parisi, and Y. C. Zhang, Phys. Rev. Lett. **56**, 889 (1986).
  - <sup>2</sup>S. F. Edwards and D. R. Wilkinson, Proc. R. Soc. London, Ser. A **381**, 17 (1982).
  - <sup>3</sup>S. Das Sarma and P. I. Tamborenea, Phys. Rev. Lett. **66**, 325 (1991); D. E. Wolf and J. Villain, Europhys. Lett. **13**, 389 (1990); J. M. Kim and S. Das Sarma, Phys. Rev. E **48**, 2599 (1993); S. Das Sarma, S. V. Ghaisas, and J. M. Kim, *ibid.* **49**, 122 (1994).
  - <sup>4</sup>Z. W. Lai and S. Das Sarma, Phys. Rev. Lett. **66**, 2348 (1991).
  - <sup>5</sup>J. Villain, J. Phys. I **1**, 19 (1991).
  - <sup>6</sup>A. Madhukar and S. V. Ghaisas, CRC Crit. Rev. Solid State Mater. Sci. **13**, 1434 (1987); A. Rockett, J. Vac. Sci. Technol. B **6**, 763 (1988); T. Kawamura, A. Kobayashi, and S. Das Sarma, Phys. Rev. B **39**, 12 723 (1989); D. D. Vvedensky and S. Clarke, Surf. Sci. **225**, 373 (1990); S. Das Sarma, J. Vac. Sci. Technol. A **8**, 2714 (1990); I. K. Marmorkos and S. Das Sarma, Phys. Rev. B **45**, 11 262 (1992), references therein.
  - <sup>7</sup>P. Smilauer, M. R. Wilby, and D. D. Vvedensky, Phys. Rev. B **47**, 4119 (1993); P. Smilauer and D. D. Vvedensky, *ibid.* **48**, 17 603 (1993); C. Ratsch, A. Zangwill, P. Smilauer, and D. D. Vvedensky, Phys. Rev. Lett. **72**, 3194 (1994).
  - <sup>8</sup>F. Family and T. Vicsek, J. Phys. A **18**, L75 (1985); F. Family, *ibid.* **19**, L441 (1986).
  - <sup>9</sup>E. A. Eklund, R. Bruinsma, J. Rudnick, and R. S. Williams, Phys. Rev. Lett. **67**, 1759 (1991); Y.-L. He, H.-N. Yang, T.-M. Lu, and G.-C. Wang, *ibid.* **69**, 3770 (1992); C. Thompson, G. Palasantzas, Y. P. Feng, S. K. Sinha, and J. Krim, Phys. Rev. B **49**, 4902 (1994); A. Iwamoto, T. Yoshinobu, and H. Iwasaki, Phys. Rev. Lett. **72**, 4025 (1994); H. Zeng and G. Vidali, *ibid.* **74**, 582 (1995).
  - <sup>10</sup>H. J. Ernst, F. Fabre, R. Folkerts, and J. Lapujoulade, Phys. Rev. Lett. **72**, 112 (1994); J. E. Van Nostrand, S. J. Chey, M.-A. Hasan, D. G. Cahill, and J. E. Greene, *ibid.* **74**, 1127 (1995); K. Thurmer, R. Koch, M. Weber, and K. H. Rieder, *ibid.* **75**, 1767 (1995).
  - <sup>11</sup>J. A. Strosio, D. T. Pierce, M. O. Stiles, A. Zangwill, and L. M. Sander, Phys. Rev. Lett. **75**, 4246 (1995).
  - <sup>12</sup>M. D. Johnson, C. Orme, A. W. Hunt, D. Graff, J. Sudijono, L. M. Sander, and B. G. Orr, Phys. Rev. Lett. **72**, 116 (1994); C. Orme, M. D. Johnson, J. L. Sudijono, K. T. Leung, and B. G. Orr, Appl. Phys. Lett. **64**, 860 (1994).
  - <sup>13</sup>H.-N. Yang, G.-C. Wang, and T.-M. Lu, Phys. Rev. Lett. **73**, 2348 (1994).
  - <sup>14</sup>G. Ehrlich and F. G. Hudda, J. Chem. Phys. **44**, 1039 (1966).
  - <sup>15</sup>R. L. Schwoebel and E. J. Shipsey, J. Appl. Phys. **37**, 3682 (1966); R. L. Schwoebel, *ibid.* **40**, 614 (1969).
  - <sup>16</sup>C. J. Lanczycki and S. Das Sarma, Phys. Rev. Lett. **76**, 780 (1996).
  - <sup>17</sup>M. Siegert and M. Plischke, Phys. Rev. Lett. **73**, 1517 (1994); Phys. Rev. E **53**, 307 (1996).
  - <sup>18</sup>A. W. Hunt, C. Orme, D. R. M. Williams, B. G. Orr, and L. M. Sander, Europhys. Lett. **27**, 611 (1994); M. Siegert, in *Scale Invariance, Interfaces, and Non-Equilibrium Dynamics*, edited by A. J. McKane, M. Droz, J. Vannimenus, and D. E. Wolf (Plenum, New York, 1995).
  - <sup>19</sup>S. Das Sarma, C. J. Lanczycki, R. Kotlyar, and S. V. Ghaisas, Phys. Rev. E **53**, 359 (1996); C. J. Lanczycki and S. Das Sarma, *ibid.* **50**, 213 (1994).
  - <sup>20</sup>S. Das Sarma, S. V. Ghaisas, and J. M. Kim, Phys. Rev. E **49**, 122 (1994); M. Schroeder, M. Siegert, D. E. Wolf, J. D. Shore, and M. Plischke, Europhys. Lett. **24**, 563 (1993).
  - <sup>21</sup>J. Krim and G. Palasantzas, Int. J. Mod. Phys. B **9**, 599D (1995).
  - <sup>22</sup>C. Y. Mou and J. W. P. Hsu, Phys. Rev. B **53**, R7610 (1996).
  - <sup>23</sup>Y.-N. Yang and E. D. Williams, Phys. Rev. Lett. **72**, 1862 (1994).
  - <sup>24</sup>M. W. Mitchell and D. A. Bonnell, J. Mater. Res. **5**, 2244 (1990).
  - <sup>25</sup>Y.-N. Yang and E. D. Williams, Phys. Rev. B **51**, 13 238 (1995).
  - <sup>26</sup>J. Aarts and P. K. Larsen, Surf. Sci. **188**, 391 (1987).
  - <sup>27</sup>R. Altsinger, H. Busch, M. Horn, and M. Henzler, Surf. Sci. **200**, 235 (1988).
  - <sup>28</sup>U. Kohler, J. E. Demuth, and R. J. Hamers, J. Vac. Sci. Technol. A **7**, 2860 (1989).
  - <sup>29</sup>M. Horn Von Hoegen and M. Henzler, Thin Solid Films **183**, 221 (1989).
  - <sup>30</sup>M. Shima, Y. Tanishiro, K. Kobayashi, and K. Yagi, J. Cryst. Growth **115**, 359 (1991).
  - <sup>31</sup>W. Shimada and H. Tochihiro, Surf. Sci. **311**, 107 (1994).
  - <sup>32</sup>Y.-N. Yang and E. D. Williams, Scanning Microsc. **8**, 781 (1995).
  - <sup>33</sup>H.-N. Yang, G.-C. Wang, and T.-M. Lu, Phys. Rev. B **51**, 14 293 (1995).
  - <sup>34</sup>B. Voigtlander and T. Weber, Phys. Rev. Lett. **77**, 3861 (1996).
  - <sup>35</sup>Y. Shigeta, J. Endo, H. Fujino, and K. Maki, Surf. Sci. **357**, 414 (1995).

- <sup>36</sup>K. Takayanagi, Y. Tanishiro, M. Takahashi, and S. Takahashi, *J. Vac. Sci. Technol. A* **3**, 1502 (1985).
- <sup>37</sup>D. Vanderbilt, *Phys. Rev. B* **36**, 6209 (1987).
- <sup>38</sup>Y.-N. Yang, E. S. Fu, and E. D. Williams, *Surf. Sci.* **356**, 101 (1996).
- <sup>39</sup>T.-M. Lu and M. G. Lagally, *Surf. Sci.* **120**, 47 (1982).
- <sup>40</sup>H.-N. Yang, T.-M. Lu, and G.-C. Wang, *Phys. Rev. B* **47**, 3911 (1993).
- <sup>41</sup>H.-N. Yang, T.-M. Lu, and G.-C. Wang, *Phys. Rev. Lett.* **68**, 2612 (1992).
- <sup>42</sup>Y. Shigeta, J. Endo, and K. Maki, *J. Cryst. Growth* **166**, 617 (1996).
- <sup>43</sup>In the  $T=280^\circ\text{C}$  and 105 BL image [Fig. 4(a)], the fraction of the surface containing pyramids looks roughly twice as large as it is due to a slight double-tip effect. The separation of the tips (roughly 50 nm) is sufficiently large to allow a good qualitative estimate of the surface's physical characteristics, although  $P_i$  in Table I and the sample size and coverage in Table II are likely quantitatively off. Our detailed images demonstrate that the basic structure in Fig. 4(a) is not an imaging artifact. The height-height correlation function and  $W(R)$  both saturate on scales much smaller than the tip separation distance ( $\xi \approx 16$  nm; Figs. 9 and 10). Hence, the double tip should not greatly influence the quantitative results in Tables III and IV (which must be upper bounds for values from the true surface morphology).
- <sup>44</sup>A. V. Latyshev, A. L. Aseev, A. B. Krasilnikov, and S. I. Stenin, *Phys. Status Solidi A* **113**, 421 (1989).
- <sup>45</sup>R. T. Tung and F. Schrey, *Phys. Rev. Lett.* **63**, 1277 (1989).
- <sup>46</sup>A. Ichimiya, T. Hahizume, K. Ishiyama, K. Motai, and T. Sakurai, *Ultramicroscopy* **42-44**, 910 (1992).
- <sup>47</sup>T. Hasegawa, M. Kohno, S. Hosaka, and S. Hosoki, *Phys. Rev. B* **48**, 1943 (1993).
- <sup>48</sup>A. Ichimiya, H. Nakahara, and Y. Tanaka, *Thin Solid Films* **281-2**, 1 (1996).
- <sup>49</sup>S. Esch, M. Hohage, T. Michely, and G. Comsa, *Phys. Rev. Lett.* **72**, 518 (1994).
- <sup>50</sup>Y.-N. Yang and E. D. Williams, *J. Vac. Sci. Technol. A* **8**, 2481 (1990).
- <sup>51</sup>Y. Yang and E. D. Williams, *Surf. Sci.* **215**, 102 (1989).
- <sup>52</sup>M. Mundschau, E. Bauer, W. Teliaps, and W. Swiech, *Philos. Mag. A* **61**, 257 (1990).
- <sup>53</sup>D. Avnir, O. Biham, D. Lidar, and O. Malcai, *Science* **279**, 39 (1998); O. Malcai *et al.*, *Phys. Rev. E* **56**, 2817 (1997).